

# A STRATEGY FOR 3D CRS PARAMETER ESTIMATION: THE TOURNEMIRE SITE CASE STUDY

H. Perroud, M. Tygel, A. Mahamat, D. Rousset

**email:** [herve.perroud@univ-pau.fr](mailto:herve.perroud@univ-pau.fr)

**keywords:** 3D CRS, parameter estimation, case study

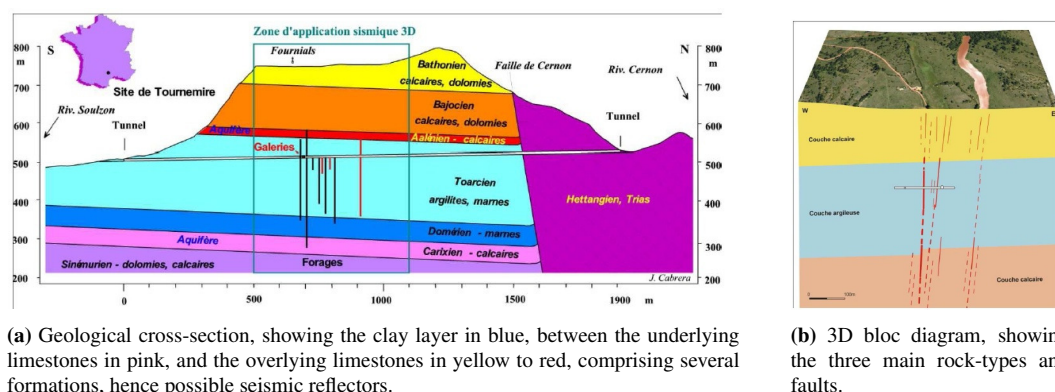
## ABSTRACT

We present here the results of CRS reprocessing of a 3D real dataset acquired in 2001 on the Tournemire site in France, which is an experimental site for the *Institut de Radioprotection et de Sûreté Nucléaire (IRSN)* to test geophysical imaging process in the context of geological nuclear waste storage. The main objective was to evaluate the ability of the methodology to recognize, in the carbonate cover of the experimental site clay layer, the prolongation of weak vertical-displacement faults seen in a tunnel within that clay layer. Previous seismic processing using the conventional common midpoint (CMP) approach did not provide satisfactory results in this cover, although the fault has been recognized in the carbonates underlying the clay layer. An original strategy was elaborated to define the best-possible parameters of the 3D Common-Reflection-Surface (CRS) stack. The procedure included refining the velocity search along a velocity guide, using a first CRS stack as the base of a subsequent curvature-parameter search, or a parameter smoothing before stacking. An optimal approach was elaborated on a subset of the data, and furthermore applied to the whole dataset. The resulting image shows improved event continuity in the carbonate cover, which allowed for horizon picking after depth migration, as well as the estimation of post-stack geometrical attributes, such as coherency. The processing indicates a zone of degraded quality of reflection events lying in the N-S direction, above the known fault zone within the underlying formations. Such feature corresponds to an alteration zone at the earth surface. Further investigation at a higher resolution scale is planned to confirm whether this zone could be a spot of possible leakage.

## INTRODUCTION

Geological (subsurface) storage is increasingly considered as a possible solution for different types of materials, including fuels, gas or nuclear wastes. It would then require efficient monitoring tools to control possible leakages of contaminated fluids from storage sites, that could represent an environment threat. Geophysical methods, and among them seismic imaging, permit a remote monitoring of storage sites, provided they are well chosen with regards to the materials under investigation and also to the needed resolution. The French *Institut de Radioprotection et de Sûreté Nucléaire (IRSN)* is developing a monitoring methodology for the geological storage of nuclear wastes, for which it has an experimental site at Tournemire, in the South-East of France. This site comprises a tunnel, previously used for train transportation, excavated into a nearly horizontal impermeable clay layer, and overlain by thick limestone formations forming a plateau (Figure 1(a)). In the tunnel, where the clay is exposed, strike-slip vertical faults are observed (Bonin, 1998), oriented in a North-South direction. The question is to evaluate whether these faults extend themselves in the carbonate cover of the tunnel, acting as possible conduits for contaminated water leakages.

In 2001, IRSN has contracted with the "Compagnie Generale de Geophysique" (CGG) for carrying out a high-resolution 3D seismic experiment, with the aim of delineating faults within the clay layer and under- and over-lying carbonates formations. After processing and interpretation, a fault was clearly identified in



(a) Geological cross-section, showing the clay layer in blue, between the underlying limestones in pink, and the overlying limestones in yellow to red, comprising several formations, hence possible seismic reflectors.

(b) 3D bloc diagram, showing the three main rock-types and faults.

**Figure 1:** Geological context of the IRSN Tournemire site, after Cabrera et al. (2001).

the lower limestone formation deeper than the clay layer. That fault corresponds well with the ones seen in the tunnel. However, due to data quality, it was not possible to recognize any fault in the clay layer itself and also in the upper limestone formations between the clay layer and the earth surface. This in spite of evidences of preferential zones of rock alteration at the surface, as shown on the bloc diagram in Figure 1(b).

Our purpose in this paper is to check whether a new imaging process like CRS stack (Jager et al., 2001) would be able to deliver, from the same data, a better image than the conventional imaging process used by CGG, in particular for fault detection in the upper limestone formations. The work was conducted from the raw data acquired in 2001, and included pre-processing, imaging and interpretation steps, using open-access software (Seismic Unix, Madagascar, OpenDTect) and the 3D CRS stack code from the Wave Inversion Technology (WIT) Consortium.

### TOURNEMIRE DATASET AND PRE-PROCESSING

The high-resolution 3D Tournemire seismic dataset comprises 863 sources at 10 m interval, laid on 20 North-South lines spaced by 50 m, which were recorded on 928 channels at 10 m interval, dispatched on 12 East-West lines, also spaced by 50 m. The exact layout, as presented in Figure 2, was positioned using differential GPS, and loaded in trace headers. The measurement surface was situated about 250 m above the tunnel, on a plateau whose elevation varies between 750 and 800 m. The source utilized was a vibroseis, with a 12 s linear sweep from 14 to 140 Hz, stacked 3 times. Each receiver group was composed of 6 10 Hz vertical geophones distributed on a 8 m array. After correlation, trace length was 2 s, with a 0.001 s sampling step, although for our target, imaging was restricted to the top 0.5 s. For imaging, the common midpoint (CMP) traces were binned in a rectangular 5 m x 5 m grid, extending on 200 bins in the East-West (in-line) direction and 120 bins in the North-South (cross-line) direction. From this rectangle, a sub-rectangle of 150 x 90 bins was extracted with a minimum CMP fold about 20. This CMP fold reaches 150 in the center part of the grid.

After vibroseis correlation, raw shots presented noise or unwanted signals of different nature (e.g., 50 Hz ringing from nearby power lines, direct air wave or surface waves, correlation artifacts, etc.). Furthermore, variable source/receiver elevations and weathering zone characteristics generated surface-consistent delays between traces. Therefore, a sequence of pre-processing steps was applied to the data in order to obtain cleaner reflection signals prior to imaging. The pre-processing sequence included muting before the first arrival and of air and surface waves, notch filtering of 50 Hz ringing, band-pass filtering, spectral balancing, and geometrical-spreading compensation. An example of a pre-processed shot gather is shown on Figure 3. We see that the reflection signals can be identified, although the signal-to-noise ratio appears to be weak in some parts of the display.

Statics corrections were applied in two steps: first, elevation statics were calculated. Next, using a preliminary normal move-out (NMO) velocity, residual statics were carried out by cross-correlation of NMO-corrected traces. NMO velocity analysis was then conducted on selected super-CMP gathers, com-

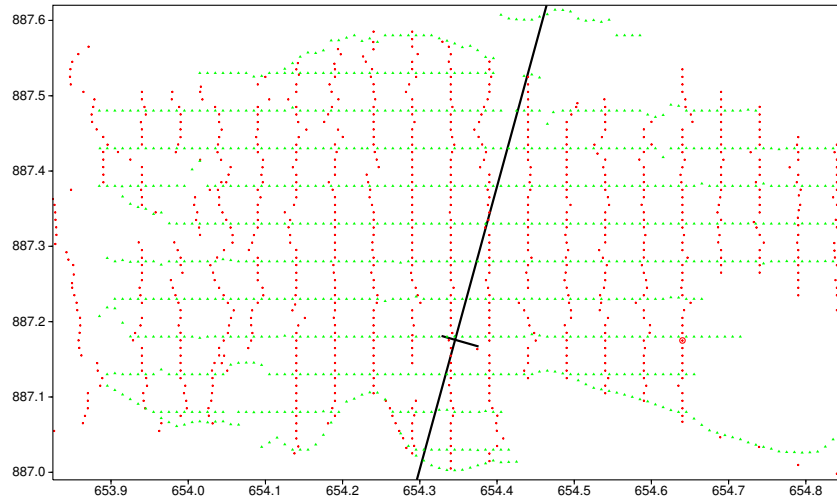


**Figure 2:** Acquisition map of sources (red) and receivers (green). The black line represents the tunnel and a gallery.

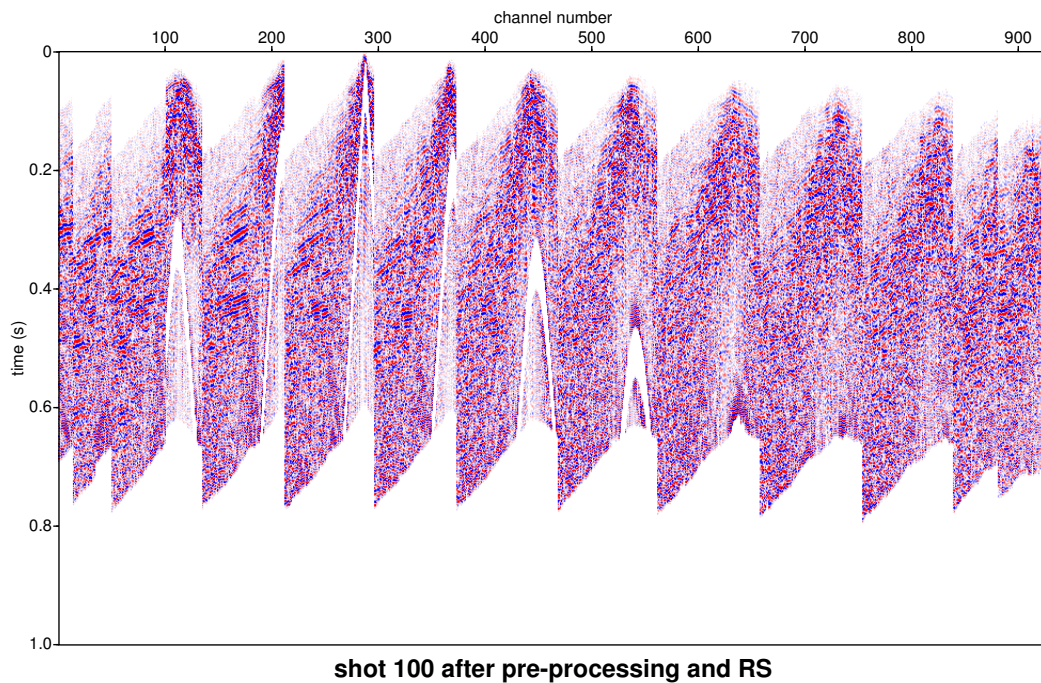


**Figure 3:** Example of a pre-processed shot gather, for the source position shown by the red circle in Figure 2 and all receivers lines.

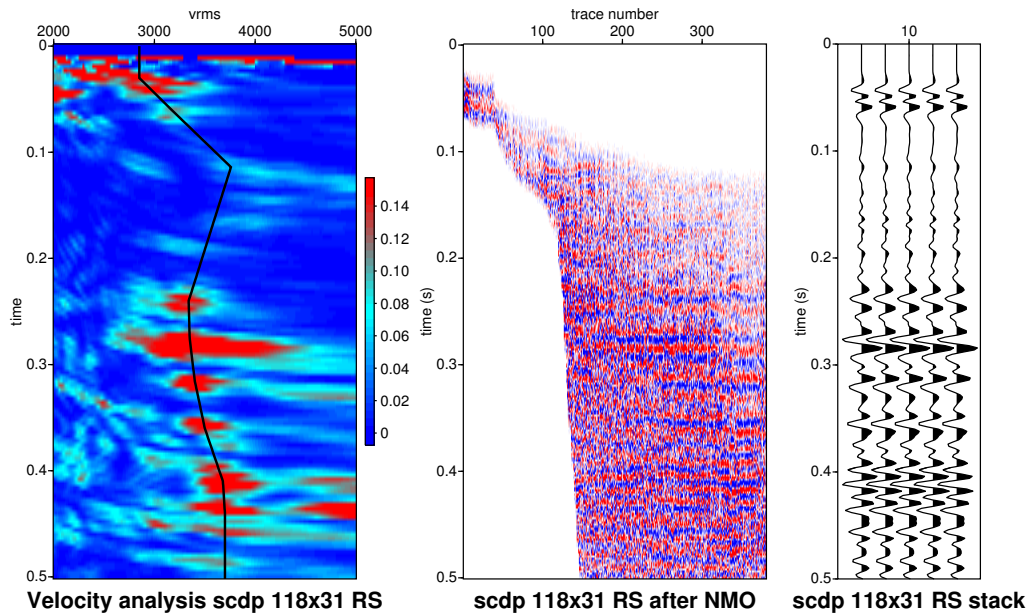


**Figure 4:** NMO velocity analysis, NMO-corrected traces and stack for an illustrative CMP gather.

posed of 3 x 3 bins (10 m x 10 m), with offsets in the range of 50 to 750 m. An example of velocity analysis, showing the semblance map, picked velocities, NMO-corrected super-gather and the corresponding stack is shown in Figure 4. The upper part of the gather had a poor offset coverage, due, for one part, to the pre-processing muting, and for the other part, to the NMO stretch mute, although quite loose (stretch mute ratio equal 2). Nevertheless, an event appears at the near surface for two-way time less than 0.1 s, while a set of clear reflection events are evidenced between 0.2 and 0.5 s. However, clear reflection events do not appear in the time range 0.1 to 0.2 s, corresponding the clay layer with the tunnel. The main objective of our CRS processing was, therefore, to provide images of such near-surface events, which could correspond to reflectivity contrasts within the upper limestone formations.

### STRATEGY FOR 3D CRS PARAMETERS ESTIMATION

The pre-processed data, re-sampled at 0.002 s over 0.6 s, and binned in CMP location for the 150 x 90 sub-rectangle, were given as the input for the 3D zero-offset (ZO) CRS stack code. In the most general way (8 independent parameters per sample and per CMP location), this corresponds to more than 30 million CRS parameters to be estimated. That task requires, of course, an efficient parameter search strategy, so as to obtain reliable results in a relatively short computation time.

The first consideration is whether the full 8 independent parameters, namely two emergence angles of the normal ray, and two 3-component symmetric curvature tensors for the NIP- and N- eigenwaves, are actually needed. As the geological context is relatively simple (gently dipping tabular sediment layers), it seemed reasonable to assume that the curvature matrices had full symmetry (local spherical wavefronts), leading to scalar (one parameter), instead of matrix (three-parameter), curvatures. In this manner, the number of independent parameters was reduced from 8 to 4, thus reducing the number of parameter estimations by a factor of two. Furthermore, curvature parameter searches were reduced from complex 3-parameter searches to much simpler 1-parameter searches.

Another way to limit the parameter-search time was to reduce the searching aperture. To do so, it was necessary to have some a priori information on the possible range of parameter variations. This was the case for the parameter search in the CMP gather (mode = cmp), since we have carried out some prior NMO velocity analysis. As it is useful to allow for some lateral velocity variations, we have, in a first step, restricted the velocity search to a range of  $\pm 500$  m/s around the mean NMO-velocities. After a first

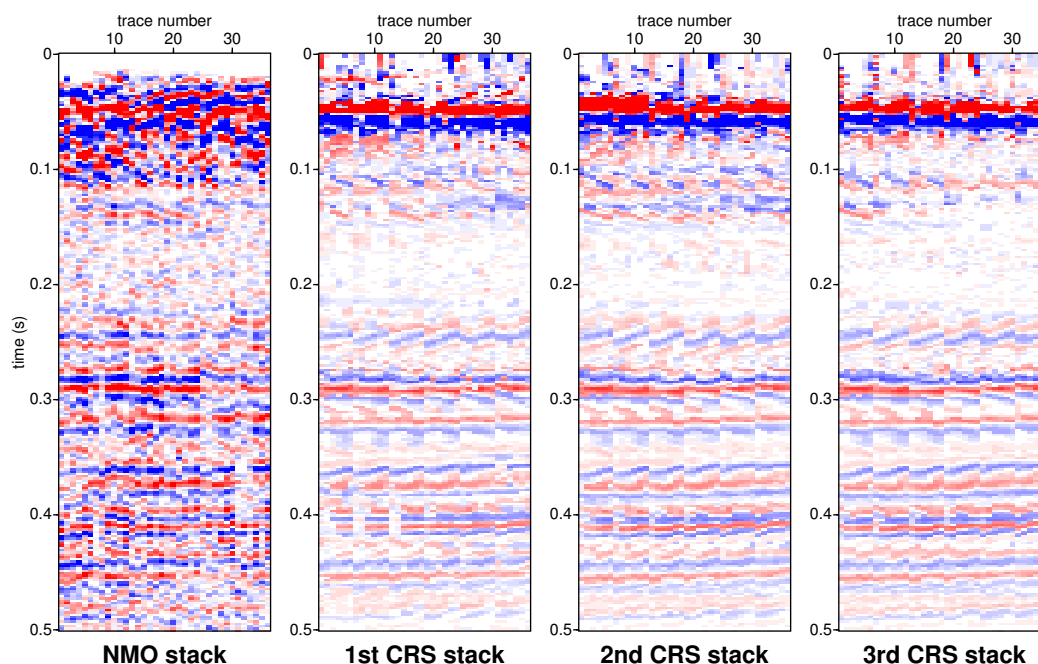


**Figure 5:** Sequence of CRS stacks obtained for the test area with successively refined parameters, compared to the CMP stack.

run of the CRS code, new velocity estimates were obtained, showing only limited lateral variations. An average time-velocity law was extracted and used as a velocity guide, with a more limited search range of  $\pm 300$  m/s, in a second CRS run.

The subsequent CRS steps (mode=zoangle and mode=zokn) implemented parameter searches in the simulated ZO (stacked) section obtained after the velocity search in the CMP gather (mode=cmp). Often, this first ZO section has a much lower quality (signal-to noise ratio, events continuity) than the optimal ZO section obtained after all parameter searches. We have, therefore, experimented searching for these parameters, not only on the CMP ZO section in the first CRS run, but also on the CRS ZO section in a second CRS run. Furthermore, we have also experimented smoothing the ZO parameters before the final CRS stack, in a third CRS run.

Altogether, we have applied these strategies in a set of 3 CRS runs for a small selected test bloc (6 x 6 bins). The corresponding CRS stacks cubes are shown unfolded in Figure 5, and compared with the conventional CMP stack. The first CRS run has the large velocity range around NMO velocities, and ZO searches in the CMP stack. The second CRS run has the narrow velocity range around the CRS velocity guide, and ZO searches in the CRS stack. The third CRS run has a further smoothing of ZO CRS parameters before CRS stacking. As the computation time increases with the number of CRS runs, we had to find the best compromise between image quality and computation cost for the processing of the whole dataset. According to the results shown in Figure 5, a clear improvement is observed between the first and second runs, in particular on the regularity of the pattern between successive cube sections. On the contrary, the third run did not seem to bring any improvement. We have therefore chosen to use the result of the second CRS run for the processing of the whole dataset. When compared with the (conventional) CMP stack results, the CRS stack provides much more focused images for the near-surface event, which is our main target here. We can therefore expect that CRS would be able to provide improved results with respect to conventional CMP, at least for the near-surface events.

The 3D CRS stack uses also aperture parameters (in offset and mid-point coordinates) and super-gather sizes that need to be chosen and tested carefully, so as to obtain reliable images. Figures 6 and 7 show the final stacked sections obtained, as inline (East-West) and cross-line (North-South) sections extracted from

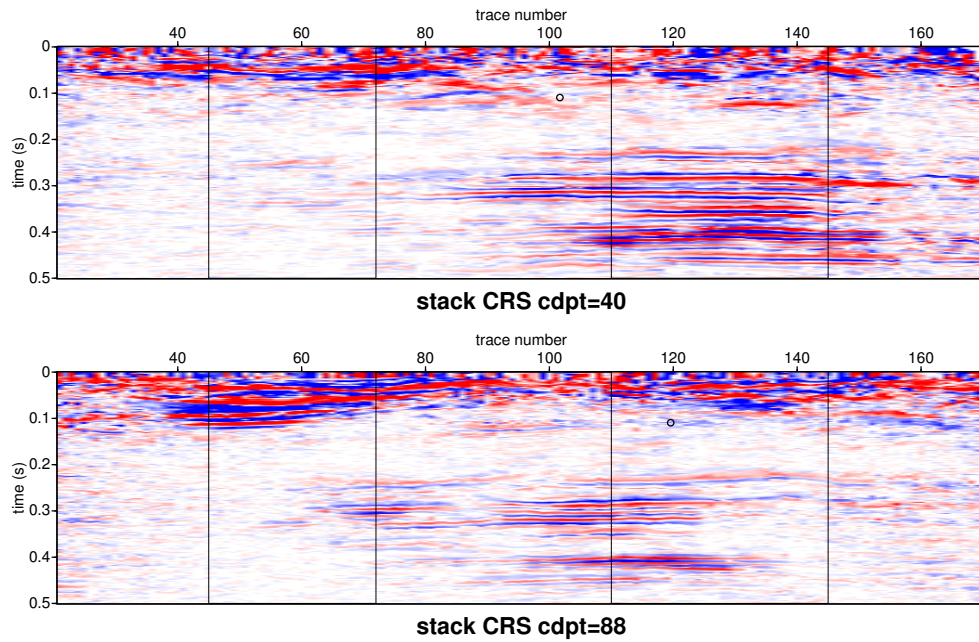


**Figure 6:** E-W inline sections of the final CRS stack cube. The vertical lines correspond to the trace of the crossline sections in Figure 7. The circles correspond to the tunnel position.

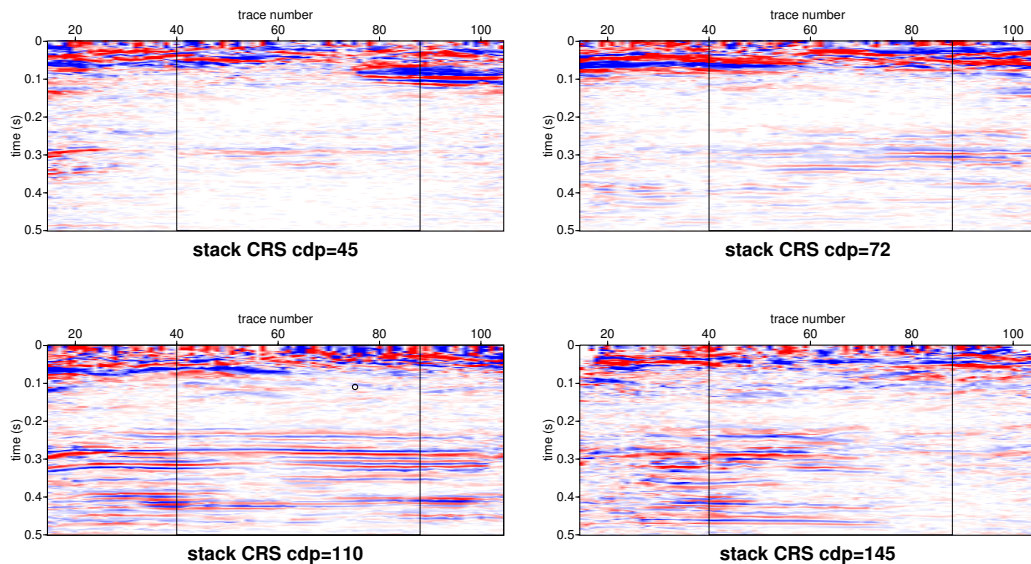


**Figure 7:** N-S crossline sections of the final CRS stack cube. The vertical lines correspond to the trace of the inline sections in Figure 6. The circles correspond to the tunnel position.

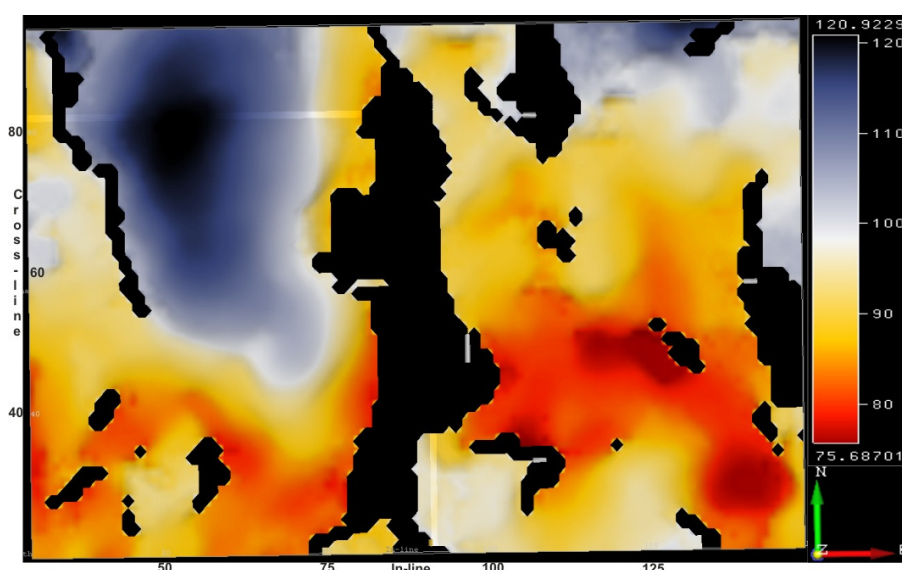


**Figure 8:** Depth map along the picked near-surface horizon. Picking was not possible in the black parts.

the stacked (simulated ZO) cube. The data quality appears very variable along the sections. Many events corresponding to the layering below the clay layer, for times greater than 0.2 s, are present in the eastern part of the bloc, and much more difficult to follow in the western part. For the near-surface layers above the clay layer, for times lower than 0.1 s, events appear in most parts of the cube. However these are not continuous, and not as well focused as the deeper events, probably in connection with the reduced fold, linked to the aperture parameters. For further interpretation of the resulting cube, post-stack time-migration and time-to-depth conversion, or post-stack depth-migration, should first be applied.

### INTERPRETATION OF CRS STACK IMAGE

In order to produce the final depth image, the building of a depth velocity model is a mandatory step. To obtain such a velocity model, we have started from the CRS attributes obtained during the final CRS stack run, namely the curvature parameter for the NIP-wave. From it, a VRMS cube (i.e. a cube of root-mean-squared (RMS) velocities) was obtained, with the same sampling in time and space coordinates than the ZO time image cube. A first 3D smoothing in time and space was applied to that velocity cube, followed by a conversion to interval velocity in depth using Dix formula (Dix, 1955). A second 3D smoothing in space was applied to obtain the final depth velocity model that was used for migration and depth conversion. The final 3D depth image was then obtained from the ZO time image cube by a split-step phase-shift depth migration (Stoffa et al., 1990), including corrections for the lateral velocity variations, although quite weak in this case.

Interpretation of the 3D depth image cube involved picking of target horizons, such as the one whose depth map is shown in Figure 8, corresponding to a near-surface event. It reveals a quite satisfying continuity of that horizon in most part of the cube, except along a N-S trend in its middle part. The position and orientation of this trend is very much similar to the known faulting geometry in the clay layer and the underlying limestone formations. It also corresponds to a local elongated depression and alteration zone at the earth surface (see the bloc diagram in Figure 1(b)).

Clear shifts in depth do not appear, even when comparing both sides of the near-surface (target) horizon depth map. Indeed, as we are in a context of strike-slip faulting, such shifts in depth due to the faulting are not expected. It was even a goal of the project to check whether or not high-resolution seismic imaging can help in detecting these type of faults, generating only very weak vertical-displacements. It seems, therefore, that CRS re-processing was able to improve the continuity of near-surface reflection events, allowing for identification of areas of degraded quality of reflection events, which could be correlated with the possible fault traces.

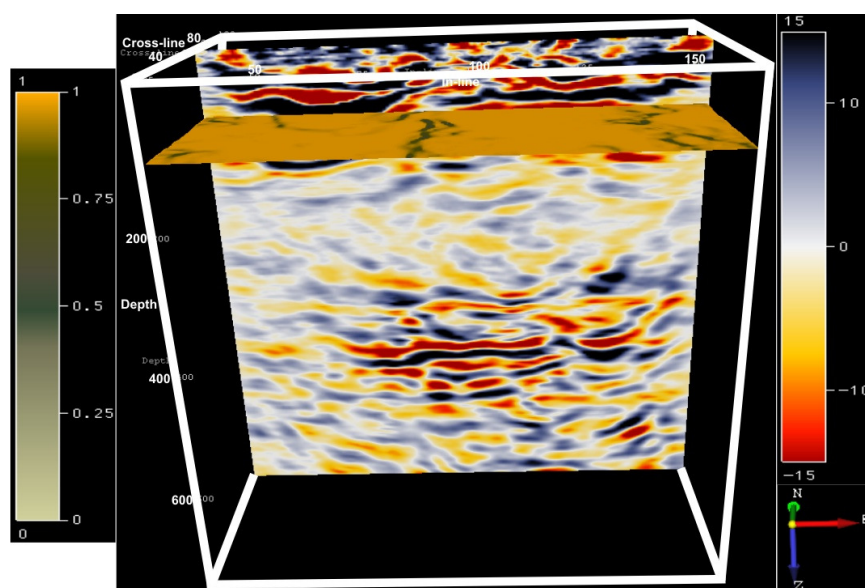


**Figure 9:** Display of coherency (grey to brown) for average near-surface horizon depth in a 3D cube view.

A further analysis of seismic geometrical attributes was conducted with the goal of trying to define more precisely the possible fault trace. Figure 9 shows the coherency attribute (Marfurt et al., 1998) measured at the average near-surface horizon depth (level 99m), in a 3D view of the depth image cube. It reveals a N-S low-coherency lineation in grey, which is a good candidate for the fault trace at this level. It is situated both inside the area without picks along the near-surface horizon, and vertically above the fault trace in the underlying limestone formations.

## CONCLUSIONS

Reprocessing of the 3D high-resolution seismic data acquired at the Tournemire site (South-East of France) has been conducted using the CRS stack imaging method. The main objective was to evaluate the ability of the methodology to recognize, in the carbonate cover of the experimental site clay layer, the prolongation of weak vertical-displacement faults seen in a tunnel within that clay layer.

The method was implemented using an elaborated strategy for optimal CRS parameter estimations. The results provided good-quality images, particularly in the near-surface part of the investigated volume. The processing indicated a zone of degraded quality of reflection events lying in the N-S direction, above the known fault zone within the underlying formations. Such feature corresponds to an alteration zone at the earth surface. Together with the velocity model constructed from the CRS attributes, the interpretation of the final depth-migrated seismic cube revealed evidences of a possible fault trace in these near-surface layers, albeit the weak vertical displacements. Further investigation at an even higher resolution scale is planned to confirm whether this zone could be a spot of possible leakage. The obtained good results indicate that the described imaging methodology can be seen as an efficient tool for geophysical monitoring of nuclear waste storage sites.

## ACKNOWLEDGMENTS

This work was initiated during HP's stay at the Laboratory of Geophysical Computing (LGC), at the State University of Campinas (UNICAMP), Brazil, in February, 2010. That work was kindly supported by the French IRSN/CNRS GNR TRASSE and the sponsors of the *Wave Inversion Technology (WIT) Consortium*. We thank IRSN for support to A.M. and fruitful discussions with J. Cabrera and C. Gelis.

---

**REFERENCES**

- Bonin, B. (1998). Deep geological disposal in argillaceous formations: studies at the tournemire test site. *Journal of Contaminant Hydrology*, 35:315–330.
- Cabrera, J., Beaucaire, C., Bruno, G., Windt, L. D., Genty, A., Ramambasoa, N., Rejeb, A., Savoye, S., and Volant, P. (2001). Projet tournemire, synthèse des programmes de recherches de 1995 à 1999. *Institut de Radioprotection et de Sécurité Nucléaire Internal Report*.
- Dix, C. H. (1955). Seismic velocities from surface measurements. *Geophysics*, 20(1):68–86.
- Jager, R., Mann, J., Hocht, G., and Hubral, P. (2001). Common reflection surface stack: image and attributes. *Geophysics*, 66:97–109.
- Marfurt, K. J., Kirlin, R. L., Farmer, S. L., and Bahorich, M. S. (1998). 3-d seismic attributes using a semblance-based coherency algorithm. *Geophysics*, 63(4):1150–1165.
- Stoffa, P., Fokkeman, J., Frere, R. D. L., and Kessinger, W. (1990). Split-step fourier migration. *Geophysics*, 55:410–421.